






RESEARCH ARTICLE

Quantitative sodium magnetic resonance imaging in food: Addressing sensitivity issues using single quantum chemical shift imaging at high field

Sylvie Clerjon^{1,2}  | Nour El Sabbagh^{1,2,3}  | Guilhem Pages^{1,2}  |
Amidou Traore^{1,2}  | Jean-Marie Bonny^{1,2} 

¹INRAE, UR QuaPA, St Genes Champanelle, France

²INRAE, PROBE Research Infrastructure, AgroResonance Facility, St Genes Champanelle, France

³Institute Pascal, Clermont Auvergne University, CHU, CNRS, Clermont Auvergne INP, Clermont-Ferrand, France

Correspondence

Sylvie Clerjon, INRAE, UR QuaPA, F-63122 St Genes Champanelle, France.
Email: sylvie.clerjon@inrae.fr

Funding information

French ANR, Grant/Award Number: ANR-19-CE21-0009; Research Council of Norway, Grant/Award Number: 269070/E50

Abstract

According to various health organizations, the global consumption of salt is higher than recommended and needs to be reduced. Ideally, this would be achieved without losing the taste of the salt itself. In order to accomplish this goal, both at the industrial and domestic levels, we need to understand the mechanisms that govern the final distribution of salt in food. The in-silico solutions in use today greatly over-simplify the real food structure. Measuring the quantity of sodium at the local level is key to understanding sodium distribution. Sodium magnetic resonance imaging (MRI), a non-destructive approach, is the ideal choice for salt mapping along transformational process. However, the low sensitivity of the sodium nucleus and its short relaxation times make this imaging difficult. In this paper, we show how sodium MRI can be used to highlight salt heterogeneities in food products, provided that the temporal decay is modeled, thus correcting for differences in relaxation speeds. We then propose an abacus which shows the relationship between the signal-to-noise ratio of the sodium MRI, the salt concentration, the B₀ field, and the spatial and temporal resolutions. This abacus simplifies making the right choices when implementing sodium MRI.

KEYWORDS

²³Na, cooked carrot, dry cured ham, food, quadripolar interactions, quantitative MRI, relaxation time, sodium MRI

1 | INTRODUCTION

Although the role that salt plays in food conservation^[1] and as a flavoring agent^[2,3] cannot be underestimated, public health organizations recommend reducing its consumption.^[4] Currently, in western countries, the elevated sodium intake strongly increases the risks for certain diseases, mostly those associated with an increase in blood pressure.^[5,6] Excessive consumption of salt is also associated with gastric cancer.^[7,8] Finally, the excessive

consumption of salt is suspected in elevating the risk of osteoporosis,^[9] kidney stones,^[10] cataracts,^[11] and type II diabetes.^[12] There exist two principal levers to diminish consumption: reducing the quantities used during industrial food production; and modifying domestic culinary practice. In order to take advantage of these two levers, it is necessary to precisely know the exact distribution of salt throughout every step of the industrial and domestic food preparation process. Understanding this distribution is necessary, both for sanitary reasons and for

organoleptic function. The reduction of salt in food must be achieved without diminishing its perception, as its taste is an essential organoleptic property of food. To this end, it is well known^[13,14] that the distribution of salt plays a crucial role in its perception. Being able to determine its location in three dimensions becomes indispensable when addressing the question of reducing salt in food. To achieve this, there exist two approaches: mathematical models and experimental measurement. Mathematical models often rely on significant oversimplification of the structure of the food product, leading to an incomplete analysis. However, there do exist some thorough, in-depth models such as a whole dried ham with bone.^[15] When a mathematical model does not exist, local measurements are used at specific moments during salt distribution. Magnetic resonance imaging (MRI) of sodium is a non-destructive tool, which allows local, 3D measurement of the concentration of sodium nuclei in an intact food. MRI is therefore the tool of choice when mapping the salt content of food throughout every stage of its production. It provides an alternative to destructive, time-consuming and spatially unresolved analysis methods such as ion chromatography.^[16,17]

Although the applications of proton MRI in food science are numerous, sodium MRI is not as common. This is principally because of the difficulties associated with the low relative sensitivity of sodium compared to the proton (0.0925) and the quadrupolar electric moment of the sodium nucleus. The relaxation of sodium is very sensitive to internal electric fields, which can cause both short and multiple T₂.^[18,19] Despite the low sensitivity of the nucleus, spatial resolution should be able to assess the spatial variations of the quantity of salt in relation to the structure of the product (e.g., the salt gradient of ham during salting is affected by the presence of fat tissue). Temporal resolution should be sufficient to track the distribution of salt during every stage of a given food process. Unfortunately, the low sensitivity of the ²³Na nucleus will of course limit the signal-to-noise ratio (SNR) and is the reason why spatial and temporal resolutions degrade when compared with ¹H.

Some researchers have already obtained results by applying sodium MRI to food products. Ishida et al. tracked salt diffusion for 6 days during the pickling of a cucumber in soybean paste.^[20] These images were captured at 6.3 T with a voxel volume of $0.8 \times 0.8 \times 8 \text{ mm}^3$ and a very high salt content (1 M). After their experiments, the authors concluded that it was necessary to develop short TE sequences in order to access the total quantity of the Na⁺ ions, especially the most bounded ones, and to use more sensitive coils. The Norwegian team at SINTEF used sodium MRI to extensively

investigate the optimization of the salting of fish, in particular studying the effect of the raw material on salt diffusion.^[21–23] In these three papers, the authors obtained images of the sodium in a fish filet from about 171 mM with field-dependent voxel volumes. The images were $1.25 \times 1.25 \times 30 \text{ mm}^3$ and $1 \times 1 \times 15 \text{ mm}^3$ at 2.35 T and $1 \times 1 \times 10 \text{ mm}^3$ at 7 T. In these studies, the sodium MRI was combined with a low-field T₂ relaxation analysis. This combination demonstrated that the mobility of certain water populations in muscle tissue increases with salting due to the alteration of interactions between water molecules and macromolecules. Intense fields of 7 T were used^[21] in order to counteract the low sensitivity of sodium and to reduce the voxel volume to $1 \times 1 \times 10 \text{ mm}^3$. In this paper, classical imaging techniques were used and the low sensitivity necessitated certain adaptations. According to Bertram 2005,^[24] when acquiring images at 2 T in a full-body scanner, the larger voxel volume of $1.9 \times 1.9 \times 40 \text{ mm}^3$ induced blurring when mapping the sodium, due to the larger thickness of the slice. All of these examples of sodium MRI applied to food products demonstrate that the voxel value may be reduced when the B₀ field is increased. Currently, this optimization is performed in a heuristic manner, on a case by case basis, as no mathematical models exist which allow us to estimate the SNR as it pertains to voxel value, B₀ field and salt concentration.

In MRI, images are obtained at a specific time (called echo time, TE), which is often non-negligible when compared to the T₂ relaxation time of sodium. Consequently, if the images are not corrected for the relaxation time, they underestimate the quantity of sodium.^[25,26] Veliyulin et al.^[27] are particularly involved in studying the question of the invisibility of the most bonded sodium, which has the fastest relaxation, in the muscle tissue of salted fish (cod and salmon). In Veliyulin study, the signal loss is corrected by assuming a mono-exponential decay of the signal. Despite this correction, invisible sodium content is non-negligible and depends on the salt concentration. Indeed, 89% of sodium is visible for the lightly salted cod, and only 22% for the heavily salted salmon. One solution to improve the visibility of the sodium nucleus while reducing the confusing effects of T₂ relaxation is to use short TE sequences, such as single point imaging (SPI) or SPRITE.^[28,29] Recently, quicker alternative short TE sequences have been introduced.^[30,31] The principle is to traverse the Fourier plane during relaxation, because spatial resolution (i.e., the point spread function [PSF]) depends on the relaxation and strongly degrades as the T₂* diminishes.

In this paper, quantitative sodium nucleus maps obtained at 4.7 T and 9.4 T were reconstructed on two food products, whose salt concentrations covered a wide

range. The two products used were a carrot cooked in slightly salted water, which presented a final salt content in the order of 100 mM, and a dry Norwegian ham with a salt content of about 800 mM. Instead of using short TE approaches, a spectroscopic method was used which allows for the acquisition of a very well resolved free induction decay (FID) in the temporal dimension without the interdependence of spatial resolution and relaxation. Although these techniques are not generally used due to their lack of speed, they are well suited to our context, where the distribution of salt is stable during image set acquisition time (approximately 2 h). To correct for the visible sodium, an AMARES model was adjusted for temporal signals.^[32] Based on the map obtained, a mathematical model was developed that allowed to link the SNR to the voxel volume, the salt concentration and the B₀ field.

2 | RESULTS AND DISCUSSION

We applied the multidimensional MRI method on our carrot and ham samples. For both samples, we compare here the raw images, and the amplitude maps resulting from the AMARES fitting. Figure 1a presents sodium MRIs obtained at 9.4 T in a carrot cooked for 25 min in boiling salted water ([NaCl] = 171 mM). The carrot is surrounded by three homogeneous reference tubes containing respectively 85, 171, and 342 mM of NaCl in gelatin. The left image is the raw MRI and the right image is the AMARES amplitude map. The first positive effect of such processing is the correction of different relaxation behavior in the reference tubes. Indeed, in Figure 1b, the relation between the FID mean signal (raw image, left) and the AMARES amplitude (right) and the salt content is compared. At 9.4 T, for our range of reference tubes, the linear model fits better with the AMARES amplitude than with the FID mean signal.

The results obtained in the carrot sample show an inhomogeneous distribution of salt concentration. The gradient in the carrot is consistent with the salting process, as the salt water permeates the carrot during the cooking process from the exterior to the interior. The concentration around the periphery (approximately 120 mM) is logically inferior to that of the salt water (171 mM). The observed salt content gradient is also congruent with absorption atomic measurements performed on similar cooked carrots (from almost 143 mM in the parenchyma to 66 mM in the carrot core). We also observed that the AMARES correction significantly highlighted the spatial differences of the concentrations, which is explained by the effect of the salt concentration on the relaxation. Indeed, an increase in sodium leads to

faster relaxation.^[27] On the non-corrected images, a signal increase due to higher nucleus density is compensated by a decay due to relaxation, and vice versa. These results demonstrate that the relaxation of the visible signal, even in the reference tubes, should not be ignored. The gradient observed in this sample (almost 120 mM in the parenchyma to 60 mM in the core) can be compared to the absorption atomic.

The same quantitative MRI protocol was applied to the second sample, a Norwegian dry cured ham at 4.7 T. Figure 2a presents raw (left) and corrected (right) sodium MRI of the whole ham surrounded by four reference tubes (2 × 513 mM and 2 × 171 mM). It should be noted that the correction does not improve sodium calibration (Figure 2b). In other words, the relaxation behaves here identically in the four reference tubes. However, AMARES correction significantly changed the measured salt content in the whole ham from 172 to 206 mM. Just as before, this result demonstrates that relaxation cannot be ignored when the imaging method leads to TE of the order of magnitude of the T₂* of the food (about 8 ms in our ham).

The absolute values of salt concentrations estimated by MRI are valid if the regime of quadrupolar interactions are equivalent in both the reference tubes and the sample. In such situation, the visible sodium fraction will be the same and the AMARES-based correction is sufficient. However, considering the diversity of the food matrices, it is critical to properly characterize the time-scale of the quadrupolar interactions to obtain an absolute sodium quantification.

Figure 2c also presents a comparison between salt content in the fat covered muscle and in the uncovered muscle (see position on Figure 2a), for the raw and for the corrected sodium MRI. The AMARES correction enables to significantly differentiate the salt content in these two parts.

These two application examples show the importance of correcting for relaxation differences in order to achieve a realistic quantitative sodium MRI. They reveal salt variations that are almost insignificant at times (a few tens of mM), but which are essential when it comes to optimizing a process for calculating the exact amount of needed salt. In our application, we significantly differentiate a sodium concentration of 171 ± 30 mM in the covered muscle between a sodium concentration of 213 ± 30 mM in the uncovered muscle. In addition to distribution, the mobility of the sodium ions plays a major role in the perception of the salt's taste. The amount of the least bonded sodium, with a mono exponential relaxation, as observed in solution, correlates both with sodium release in saliva and salt perception.^[33,34] The CSI method used here also has the benefit of being able to measure the local T₂*

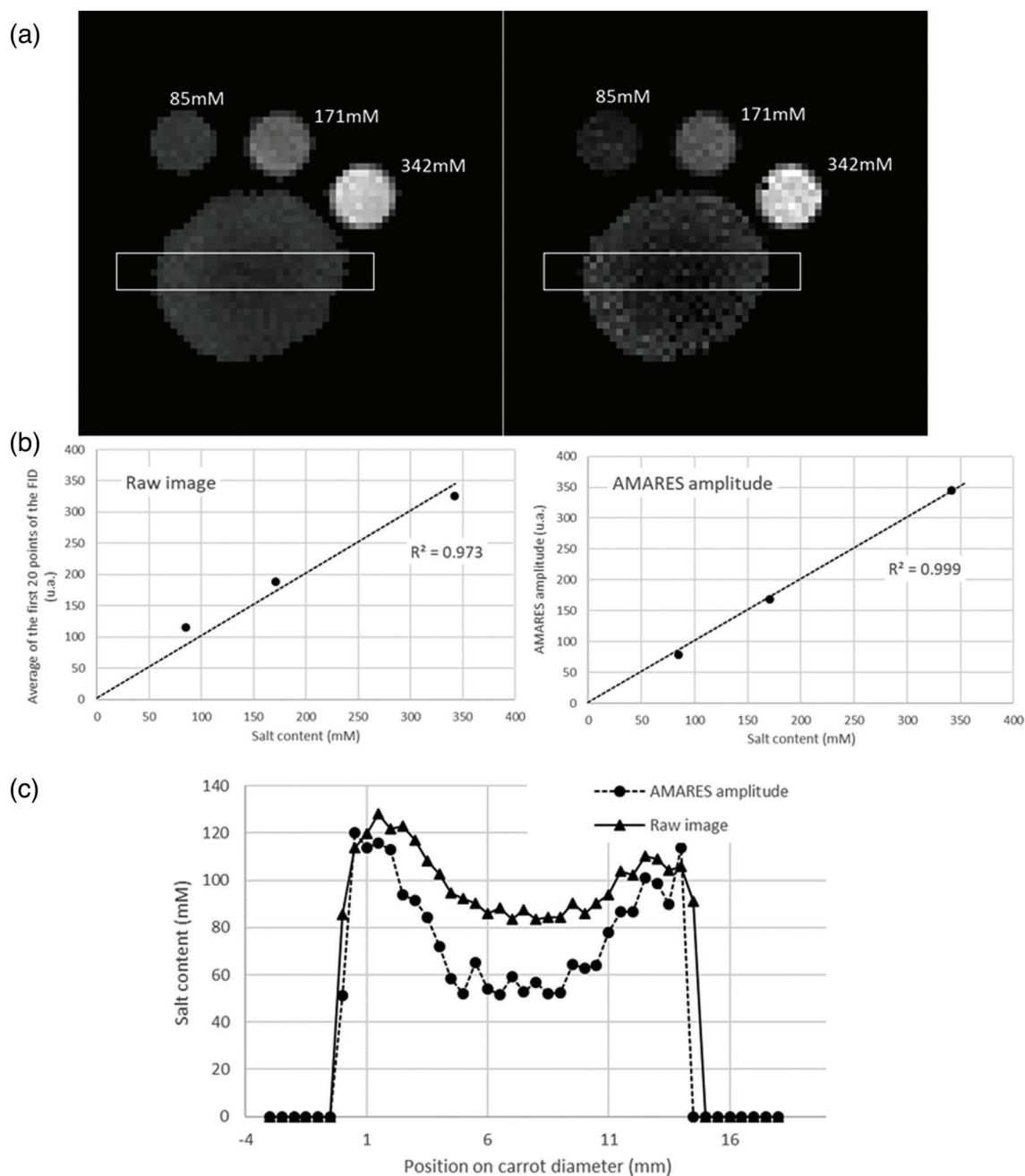


FIGURE 1 Effect of AMARES correction on the sodium magnetic resonance imaging (MRI) of the carrot sample. (a) Raw (left) and corrected (right) sodium MRI, (b) linear relationship between the nuclear magnetic resonance (NMR) signal and the salt content in the reference tubes, before (left) and after (right) correction, (c) salt content profile in the carrot before and after correction

which gives a general idea of the mobility of the sodium nucleus.

Apart from the relaxation differences and B_0 heterogeneities discussed here, other biases exist when it comes to quantifying sodium, such as the heterogeneities of the RF $B_1 +$ field in the sample. These heterogeneities are all the greater when the B_0 field is high (and then wavelengths are short). It is possible to quantify and correct the $B_1 +$ field.^[35,36] However, these approaches were mainly implemented in ^1H . It remains to be checked that

the improvement in systematic error is not offset by an increase in uncertainty, as it is likely that the $B_1 +$ maps obtained in sodium are highly affected by noise propagation.

In addition to correcting for relaxation effects, because of the low sensitivity of the sodium nucleus, it is particularly important in sodium MRI to adjust the volume of the voxel to obtain sufficient SNR. Rather than proceeding by heuristic optimization, an abacus is introduced here giving, at 4.7 and 9.4 T, the relationship

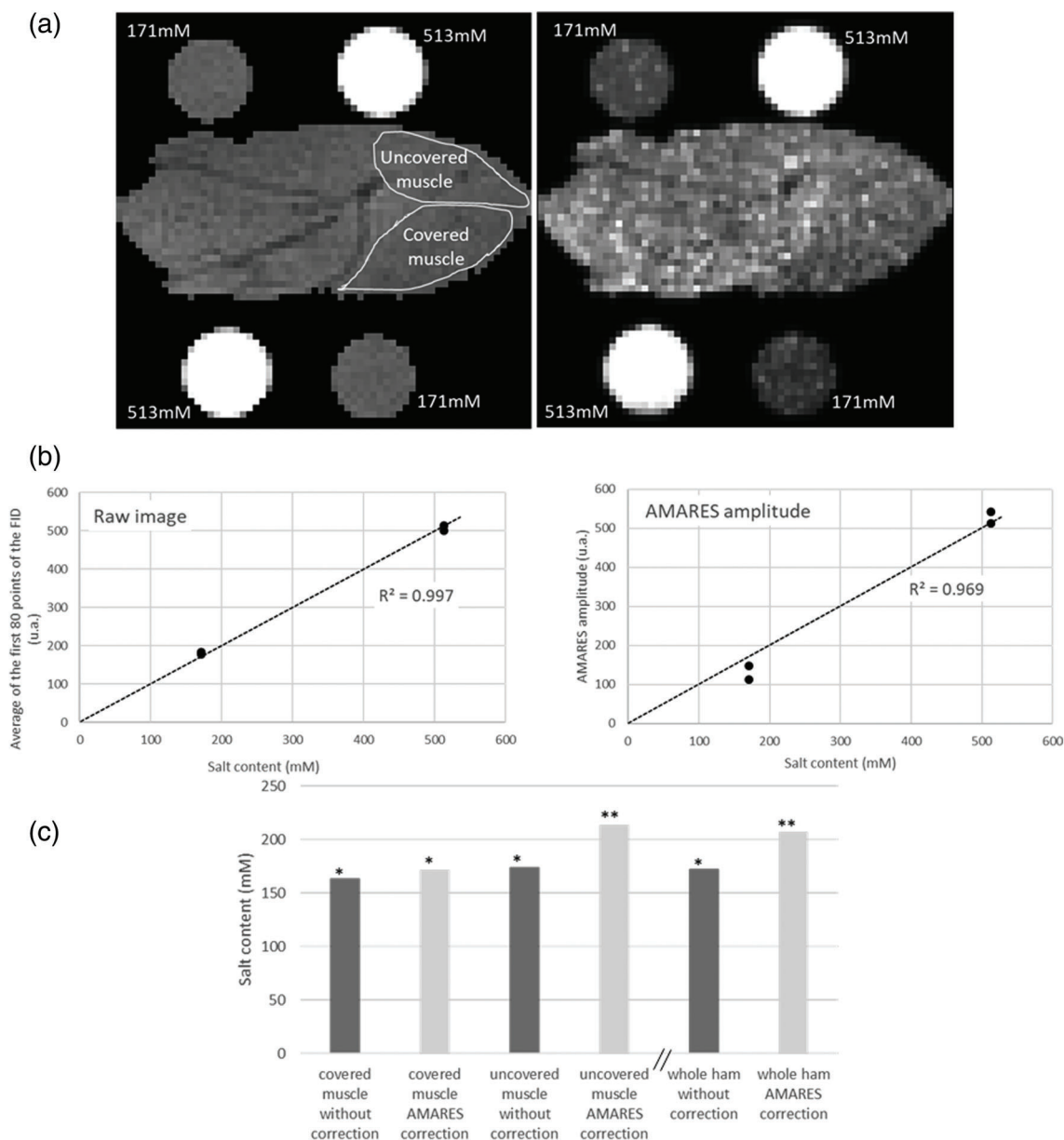


FIGURE 2 Effect of AMARES correction on the sodium MRI of the ham sample. (a) Raw (left) and corrected (right) sodium MRI, (b) linear relationship between the nuclear magnetic resonance (NMR) signal and the salt content in the reference tubes, before (left) and after (right) correction, (c) salt content measurement in the covered muscle, uncovered muscle and in the whole ham, with and without correction

between SNR and sodium concentration, after normalization of the volume of the voxel (Figure 3).

As expected, this relation is linear for both B_0 :

$$\text{At } 9.4 \text{ T} \quad \text{SNR} = 27.60 \times \sqrt{N} \times \text{voxel.volume} \times [\text{Na}]$$

$$\text{At } 4.7 \text{ T} \quad \text{SNR} = 0.56 \times \sqrt{N} \times \text{voxel.volume} \times [\text{Na}]$$

The results show a considerable increase in sensitivity when increasing the B_0 from 4.7 T to 9.4 T. Indeed, the sensitivity ratio is almost 60. This ratio can be explained by the nuclear polarization boost due to the B_0 increase but also by the difference of experimental conditions. The filling factors were different. At 9.4 T, the sample fully

filled the 3 cm of the coil while at 4.7 T, the ham is only 12 cm (in plan) for a 20-cm coil (internal diameter). The filling ratio effect seemed to be more influent here than coil geometry factors and polarization (birdcage, linear polarization at 9.4 T vs. Litzcage, quadratic polarization at 4.7 T). However, other experimental factors could cause this sensibility difference. For instance, noise levels caused by the sample, by the coil and the receiver chain, which depend on the magnetic field.^[37] In sum, it is important to note that the slope of each linear model presented on Figure 3 is specific to a hardware configuration. If the configuration is unchanged, which is often the case in practice, they can then be used for predicting the SNR of MRI acquisitions.

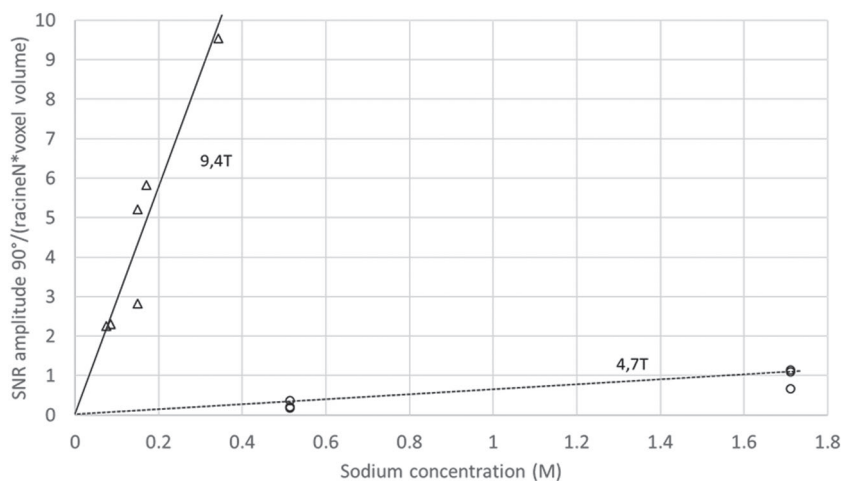


FIGURE 3 Abacus giving the relationship between resolution, salt content and signal-to-noise ratio (SNR), in sodium magnetic resonance imaging (MRI), at 4.7 and 9.4 T

These results allow to extrapolate the experimental conditions necessary to image sodium in a given salted sample. Consider a food product with a realistic salt content of 0.17 M (almost 1 g of NaCl for 100 g of food product). Using a 9.4-T MRI device and a sample small enough to enter the coil, SNR = 10 can be expected in a 1 h 16 min total acquisition duration for an isotropic voxel volume at 1 mm³. If a higher spatial resolution in plane is needed, for instance 0.5 × 0.5 with a slice thickness at 1 mm, the total duration becomes 4 h 50 min. At 4.7 T, the same SNR conditions can be obtained in 1 h 30 min with 2 × 2 × 4 mm³ voxel geometry. The improvement to 1*1*4 mm³ lengthens the total acquisition duration to 6 h.

In this experiment, priority is given to obtaining temporal information. This is done in order to precisely adjust the relaxation and to optimize the spatial resolution, at the cost of an increase of the initial TE (~1 ms at 9.4 T, 5.4 ms at 4.7 T). Thus, correcting for relaxation becomes a key point, whose efficiency relies on the quality of the modeling. Here the quality of the Lorentzian adjustment is validated by verifying that the average deviation between the data and the model is explained by the SNR levels in the entire image. However, such a correction made on the observable sodium component does not guarantee that a significant part of the sodium was not relaxed during TE. This may be the case if the quadrupolar interactions are not null in the food products, which would lead to a bi-exponential behavior of the T2 relaxation. This relaxation analysis is not discussed here as it requires specific nuclear magnetic resonance (NMR) spectroscopic approaches. For more detailed information, it is possible to refer to the complementary work carried out by our group in El Sabbagh et al.^[38]

The value of short TE approaches for mapping sodium cannot be overlooked as they guarantee the visibility of sodium in its entirety. It should be noted that the TE obtained is short, although never zero. Radial, as well as spiral trajectories in place of Cartesian k-space filling are well-known solutions, but they lead to interactions

between relaxation and PSF whose consequences on quantification are difficult to evaluate.^[30,31] This recent study goes further by using anisotropic radial filling, which takes advantage of the object shape, here elongated tissue such as muscle.

The difference in sensitivity observed between 4.7 T and 9.4 T suggests that RF coil optimization plays a key role. The relative size of the coil with respect to the sample size must be chosen to optimize the filling ratio. Moreover, RF coils should be able to support a large field of-view (FOV) with high radio frequency (RF) field homogeneity in transmission and to achieve high SNR in reception.^[37] Up to date, antennas take advantage of RF simulation tools for their conception and manufacturers provide high-quality devices, and adapt, when necessary, the coil geometry for particular needs. In conclusion, it is clear that a B0 enhancement, for a given FOV, is a direct solution to improve SNR. Even if such high field MRI is not without its difficulties, such as RF and B0 heterogeneities, many publications highlight the advantages of ultra-high field sodium MRI, mainly at 7 T.^[39,40] Magnet manufacturers and scientists are working on both superconductivity improvements^[41,42] and cryogen-free MRI solutions^[43] to build the next generation of devices.

3 | EXPERIMENTAL

3.1 | Samples

The first sample was a peeled carrot cultivar (*Daucus carota* subsp. *Sativus*, local purchase) length 8 cm, diameter 2 cm (weight = 24 g) cooked for 25 min in boiling salted water ([NaCl] = 171 mM). The carrot was surrounded by three reference tubes containing respectively 85, 171, and 342 mM of NaCl in gelatin from porcine skin (5% in weight, gel strength 300, Type A, Sigma).

The second sample was a 3-kg entire Norwegian dry cured ham (length 33 cm, width 12 cm, height 8 cm).

The ham was surrounded by four reference tubes divided in two groups containing respectively 0.513 and 1.71 M of NaCl in gelatin from porcine skin (5% in weight, gel strength 300, Type A, Sigma).

Three other reference tubes were used for the abacus construction at 9.4 T. One tube consisted of 150 mM of NaCl and 1-mM CuSO₄ in gelatin from porcine skin (5% in weight, gel strength 300, Type A, Sigma), one tube consisted in 150 mM of NaCl and 1-mM CuSO₄ in agar gel (1.5% w/w, Noble Agar, Sigma-Aldrich) and the last tube consisted of 75 mM of NaCl and 0.5-mM CuSO₄ in agar gel (1.5% w/w, Noble Agar, Sigma-Aldrich).

The salted gelatin production process makes sure that sodium concentration is homogeneous in all our reference tubes. Indeed, the process consisted in complete dissolution of NaCl in water heated at 60°C and then a complete dissolution of gel or agar in salted water, at 60°C. The full process lasted 20 min with a continuous stir.

3.2 | MRI

Carrot investigations were performed on a 9.4 T Bruker Ascend 400WB instrument (Bruker, Ettlingen, Germany) equipped with a microimaging accessory and using a 32-mm diameter linear ¹H/²³Na birdcage radiofrequency Bruker coil used for both excitation and signal reception at 106 MHz for sodium.

For the entire ham, investigations were performed on a horizontal Biospec 4.7 T MRI system (Bruker GmbH, Ettlingen, Germany), equipped with a BGA-26 gradient system and a Doty (DOTY Scientific Inc., Columbia, USA) quadrature-polarized coil (¹H/²³Na) for both emission and signal reception at 53 MHz for sodium.^[44]

The MRI method is based on the chemical shift imaging (CSI) approach introduced by Brown et al.^[45] It is based on a Cartesian path of the 2D Fourier plane using gradient pulses in the *x* and *y* directions (i.e., phase encoding steps) and a selective excitation of a thick slice in the *z* direction. Shinnar-Le Roux (SLR) type selective pulses are calibrated at 90°. For a given slice, the information is multidimensional, because an FID signal is obtained in each voxel. The FID sampling started at TE and had a high temporal resolution (Table 1).

3.3 | Post-processing

In each voxel, the FID signal was adjusted with the AMARES approach.^[32] The principle was to fit the time-domain FID signal in each voxel with an exponentially dampened sinusoid (i.e., Lorentzian lines after Fourier transform). This fitting provided four-parameter estimates of amplitude *a*, damping $d = 1/T_2^*$, frequency offset and phase shift. This adjustment was performed in several steps. First, parameter guesses were obtained separately, then all the parameters were estimated in the least-squares sense based on the complex time-domain data. The quality of this adjustment is shown in the supporting information. The main benefit of this approach was the ability to control the quality of the mono-exponential relaxation model on many points in order to obtain an amplitude that was corrected for the effects of relaxation as well as for B0 inhomogeneities. To highlight the effect of AMARES correction, amplitude maps were compared to the raw images. Raw images were obtained from the CSI acquisitions by averaging the first points of the FID; for the carrot, the first 20 points out of 2048 were averaged, for the ham, the first 80 points out of 8192 were averaged.

The final stage consisted in converting the amplitude map obtained by AMARES into a volumetric concentration map. To this end, the average AMARES amplitude *a_i* in each reference tube was measured in a region of interest centered on the center of tubes and small enough to avoid side effects. A linear model $a_i = k[\text{concentration}]_i$ was adjusted in order to link these amplitudes with previously known reference tubes volumetric concentrations. The final concentration map was generated by dividing the amplitude map by the obtained *k* coefficient. The same conversion steps were performed on the raw image.

The SNR of the AMARES amplitude *a* map was also mapped. This parameter indicated the achieved amplitude in relation to the propagated noise levels in the map acquired by AMARES. It is based on the Cramér–Rao lower bound for a single peak,^[46] which provides an algebraic expression of the minimal standard deviation (SD) of the estimated amplitude

TABLE 1 CSI sequence details for 9.4 and 4.7 T sodium magnetic resonance imaging (MRI) acquisitions

B0 (T)	Object	In plane vox. size (mm)	Slice thickness (mm)	Temporal resol. (μs)	TE/TR (ms/ms)	Total duration
9.4	Carrot and tubes	0.5 × 0.5	8	12	0.95/500	1 h 30 min
4.7	Ham and tubes	2 × 2	8	5	5.4/200	2 h 15 min

$$\text{CRB}_a = 2\sqrt{-\hat{d}t_s\sigma}$$

where t_s is the temporal resolution given in the Table 1 and σ is the SD of noise affecting the FIDs. σ is obtained by calculating the SD of the terminal part of the complex FID, as this is the only part where noise is expressed. In each voxel the SNR is obtained as follows:

$$\text{SNR} = \hat{a}/\text{CRB}_a$$

The mean SNR was measured in each reference tube. Then each SNR measurement is normalized by $(\sqrt{N} \times \text{voxel volume})$, N being the accumulation factor during acquisition. These measurements were represented as a function of the known salt concentration.

ACKNOWLEDGMENTS

Thanks to Cécile Leroy for her conscientious work on sodium MRI acquisitions and treatment.

These results have been presented during the online Workshop on the Applications of Magnetic Resonance in Food Science: Multiscale Food Structures and FoodOmics, October 28–29, 2021. The video of this presentation is available online (with the DOI: 10.5281/zenodo.5644833).

This study has been funded by the two following projects: Express, a project funded by the Research Council of Norway, 269070/E50, 2017–2020. French ANR project Sal&Mieux ANR-19-CE21-0009, 2020–2024.

PEER REVIEW

The peer review history for this article is available at <https://publons.com/publon/10.1002/mrc.5239>.

ORCID

Sylvie Clerjon  <https://orcid.org/0000-0002-6273-200X>

Nour El Sabbagh  <https://orcid.org/0000-0001-5100-3429>

Guilhem Pages  <https://orcid.org/0000-0001-9368-5237>

Amidou Traore  <https://orcid.org/0000-0002-3574-3475>

Jean-Marie Bonny  <https://orcid.org/0000-0003-2858-7459>

REFERENCES

- [1] J. N. Sofos, *J. Food Saf.* **1984**, 6(1), 45.
- [2] M. Leshem, *Neurosci. Biobehav. Rev.* **2009**, 33(1), 1.
- [3] D. G. Liem, F. Miremadi, R. S. J. Keast, *Nutrients* **2011**, 3(6), 694.
- [4] World Health Organization, *Global action plan for the prevention and control of noncommunicable diseases*, World Health Organization, Geneva **2013** 2013.
- [5] H. O. Dickinson, J. M. Mason, D. J. Nicolson, F. Campbell, F. R. Beyer, J. V. Cook, B. Williams, G. A. Ford, *J. Hypertens.* **2006**, 24(2), 215.
- [6] F. M. Sacks, L. P. Svetkey, W. M. Vollmer, L. J. Appel, G. A. Bray, D. Harsha, E. Obarzanek, P. R. Conlin, E. R. Miller, D. G. Simons-Morton, N. Karanja, P. H. Lin, D. A.-S. C. R. Grp, *N. Engl. J. Med.* **2001**, 344(1), 3.
- [7] P. Correa, *Cancer Res.* **1992**, 52(24), 6735.
- [8] W. G. Yang, C. B. Chen, Z. X. Wang, Y. P. Liu, X. Y. Wen, S. F. Zhang, T. W. Sun, *World J. Gastroenterol.* **2011**, 17(15), 2049.
- [9] A. Devine, R. A. Criddle, I. M. Dick, D. A. Kerr, R. L. Prince, *Am. J. Clin. Nutr.* **1995**, 62(4), 740.
- [10] F. P. Cappuccio, R. Kalaitzidis, S. Duneclift, J. B. Eastwood, *J. Nephrol.* **2000**, 13(3), 169.
- [11] A. Tavani, E. Negri, C. LaVecchia, *Ann. Epidemiol.* **1996**, 6(1), 41.
- [12] G. Hu, P. Jousilahti, M. Peltonen, J. Lindstrom, J. Tuomilehto, *Diabetologia* **2005**, 48(8), 1477.
- [13] M. Emorine, C. Septier, T. Thomas-Danguin, C. Salles, *Int. Food Res.* **2013**, 51(2), 641.
- [14] A. Syarifuddin, C. Septier, C. Salles, T. Thomas-Danguin, *Food Qual. Prefer.* **2016**, 48(Part A), 59.
- [15] R. Harkouss, C. Chevarin, J. D. Daudin, J. Sicard, P. S. Mirade, *J. Food Eng.* **2018**, 218, 69.
- [16] P. S. Mirade, S. Portanguen, J. Sicard, J. De Souza, A. Musavu Ndob, L. C. Hoffman, T. Goli, A. Collignan, *J. Food Eng.* **2020**, 265, 109686.
- [17] J. H. Sherman, N. D. Danielson, J. W. Hazey, *J. Agric. Food Chem.* **1988**, 36(5), 966.
- [18] G. Madelin, J. S. Lee, R. R. Regatte, A. Jerschow, *Prog. Nucl. Magn. Reson. Spectrosc.* **2014**, 79, 14.
- [19] W. D. Rooney, C. S. Springer, *NMR Biomed.* **1991**, 4(5), 209.
- [20] N. Ishida, T. Kobayashi, H. Kano, S. Nagai, H. Ogawa, *Agric. Biol. Chem.* **1991**, 55(9), 2195.
- [21] I. G. Aursand, U. Erikson, E. Veliyulin, *Food Chem.* **2010**, 120(2), 482.
- [22] I. G. Aursand, E. Veliyulin, U. Bocker, R. Ofstad, T. Rustad, U. Erikson, *J. Agric. Food Chem.* **2009**, 57(1), 46.
- [23] U. Erikson, E. Veliyulin, T. Singstad, M. Aursand, *J. Food Sci.* **2004**, 69(3), FEP107.
- [24] H. C. Bertram, S. J. Holdsworth, A. D. Whittaker, H. J. Andersen, *J. Agric. Food Chem.* **2005**, 53(20), 7814.
- [25] J. P. Renou, S. Benderbous, G. Bielicki, L. Foucat, J. P. Donnat, *Magn. Reson. Imaging* **1994**, 12(1), 131.
- [26] C. Vestergaard, J. Risum, J. Adler-Nissen, *Meat Sci.* **2005**, 69(4), 663.
- [27] E. Veliyulin, I. G. Aursand, *J. Sci. Food Agric.* **2007**, 87(14), 2676.
- [28] E. Veliyulin, I. G. Aursand, U. Erikson, B. J. Balcom, Sodium MRI as a tool for optimization of salting processes, in *Magnetic Resonance in Food Science: Challenges in a Changing World*, RSC Publishing, UK **2009** 251.
- [29] E. Veliyulin, B. Egelanddal, F. Marica, B. J. Balcom, *J. Agric. Food Chem.* **2009**, 57(10), 4091.
- [30] S. Nielles-Vallespin, M. A. Weber, M. Bock, A. Bongers, P. Speier, S. E. Combs, J. Wöhrle, F. Lehmann-Horn, M. Essig, L. R. Schad, *Magn. Reson. Med.* **2007**, 57(1), 74.

- [31] M. Utzschneider, M. Muller, L. V. Gast, S. Lachner, N. G. R. Behl, A. Maier, M. Uder, A. M. Nagel, *Magn. Reson. Imaging* **2021**, 75, 72.
- [32] L. Vanhamme, A. van den Boogaart, S. Van Huffel, *J. Magn. Reson.* **1997**, 129(1), 35.
- [33] L. Boisard, I. Andriot, C. Martin, C. Septier, V. Boissard, C. Salles, E. Guichard, *Food Chem.* **2014**, 145, 437.
- [34] A. C. Mosca, I. Andriot, E. Guichard, C. Salles, *Food Hydrocoll.* **2015**, 51, 33.
- [35] M. Bouhrara, J. M. Bonny, *Magn. Reson. Med.* **2012**, 68(5), 1472.
- [36] R. Pohmann, K. Scheffler, *NMR Biomed.* **2013**, 26(3), 265.
- [37] G. Giovannetti, A. Flori, N. Martini, R. Francischello, G. D. Aquaro, A. Pingitore, F. Frijia, *Electronics* **2021**, 10(15), 1788.
- [38] N. El Sabbagh, J. M. Bonny, S. Clerjon, C. Chassain, G. Pages, Characterization of the sodium binding state in several food products by ^{23}Na NMR spectroscopy, Submitted in Magnetic Resonance in Chemistry, special issue Multiscale Food Structures and FoodOmics, **2021**.
- [39] F. Maggiorelli, G. Buonincontri, A. Retico, J. D. Kaggie, M. J. Graves, L. Biagi, G. Tiberi, M. Tosetti, *Sodium imaging of the human knee cartilage with Magnetic Resonance at Ultra High Field: development of a double frequency (H-1/Na-23) RF coil*, International Applied Computational Electromagnetics Society Symposium - Italy, New York, Ieee **2017**.
- [40] B. Ridley, A. M. Nagel, M. Bydder, A. Maarouf, J. P. Stellmann, S. Gherib, J. Verneuil, P. Viout, M. Guye, J. P. Ranjeva, W. Zaaraoui, *Sci. Rep.* **2018**, 8, 12.
- [41] H. Maeda, Y. Yanagisawa, *IEEE Trans. Appl. Supercond.* **2014**, 24(3), 1.
- [42] A. H. Xu, Y. J. Zhu, J. W. Wang, W. N. Chang, Y. F. Zhang, Y. L. Zhang, Q. H. Wang, H. J. Zou, K. H. Wu, C. Dai, Y. Shi, Y. Wu, X. G. Wang, J. Liu, X. W. Wang, F. H. Cai, *IEEE Trans. Appl. Supercond.* **2021**, 31(8), 1.
- [43] I. Saniour, G. Authelet, B. Baudouy, R. M. Dubuisson, L. Jourdain, G. Willoquet, L. Darrasse, J. C. Ginefri, M. Poirier-Quinot, *Rev. Sci. Instrum.* **2020**, 91(5), 055106.
- [44] F. D. Doty, G. N. Doty, S. Deese, S. Spitzmesser, D. Arcos, D. McCree, L. Holte, P. D. Ellis, J. M. Bonny, S. Clerjon, A Large Segmented Double-Tuned Quadrature High-field MR Coil With Exceptional Tuning Stability, 59th ENC Conference, poster 330, Orlando **2018**.
- [45] T. R. Brown, B. M. Kincaid, K. Ugurbil, *PNAS* **1982**, 79(11), 3523.
- [46] S. Cavassila, S. Deval, C. Huegen, D. van Ormondt, D. Graveron-Demilly, *J. Magn. Reson.* **2000**, 143(2), 311.

SUPPORTING INFORMATION

Additional supporting information may be found in the online version of the article at the publisher's website.

How to cite this article: S. Clerjon, N. El Sabbagh, G. Pages, A. Traore, J.-M. Bonny, *Magn Reson Chem* **2022**, 1. <https://doi.org/10.1002/mrc.5239>